Minority carrier lifetime of Ge film epitaxially grown on a large-grain seed layer on glass

T. Nishida, M. Nakata, T. Suemasu, and K. Toko [a)]

Institute of Applied Physics, University of Tsukuba, 1-1-1 Tennodai, Tsukuba, Ibaraki 305-8573, Japan

[a)] Author to whom correspondence should be addressed.
Electronic mail: toko@bk.tsukuba.ac.jp

Keywords: Metal-induced crystallization; Layer exchange; Polycrystalline films; Semiconducting germanium; Epitaxy

Abstract

To develop high-efficiency multijunction solar cells onto inexpensive substrates, an innovative technique for growing a large-grained Ge layer on glass is strongly desired. We investigated the epitaxial growth of a light absorbing Ge flim (500-nm thickness) on a large-grained (> 100 μm) Ge seed layer (50-nm thickness) formed on glass by Al-induced layer exchange. After examining molecular beam epitaxy (MBE) and solid-phase epitaxy (SPE) for both methods, Ge layers with a low Al concentration were epitaxially grown at 350 °C. Microwave photoconductivity decay revealed that the MBE-Ge layer exhibited a short minority carrier lifetime owing to the rough surface. Conversely, the SPE-Ge layer was relatively flat and exhibited a long bulk minority carrier lifetime (5.6 μs), which is close to that of a single-crystal Ge. Therefore, the seed layer concept that combines SPE with Al-induced layer exchange is a promising way for fabricating ideal bottom cells for high-efficiency multijunction solar cells based on inexpensive substrates.

I. INTRODUCTION

Multijunction solar cells have updated the highest conversion efficiency of solar cells. Ge has been used in the bottom cell of the multi-junction solar cells because of its desirable characteristics, such as its narrow band gap (0.66 eV), high absorption coefficient (~10^4 cm^{-1} at 0.8 eV), and good lattice matching to group III-V compound semiconductors (0.1% lattice mismatch with GaAs) [1,2]. However, bulk Ge substrates are expensive, which has limited their application to special uses. One promising approach to reducing the fabrication cost is substituting the bulk Ge substrate with a Ge thin film on an inexpensive glass substrate (softening temperature: ~550 °C) [3]. Additionally, (111)-oriented Ge is favorable for forming silicide solar cell materials [4] and nanowire arrays [5], which may improve solar cell performance. Transferring single-crystal Ge layers to inexpensive substrates is a promising method [6–8]; however, there remain difficulties in keeping the process costs low and fabricating in large areas.

In line with this, the low-temperature synthesis of polycrystalline (poly-) Ge on glass has been investigated using solid-phase crystallization (SPC) [9–11], sputtering [12], and chemical vapor deposition (CVD) [13,14]. Metal-induced layer exchange, using Al [15–19], Au [20,21], and Ag [22,23] as catalysts, is a unique method that significantly lowers the crystallization temperature of amorphous (a-) Ge (≤ 350 °C). In particular, Al-induced layer exchange (ALILE) allows for large-grained (> 50 µm), (111)-oriented, and highly p-doped Ge thin films (thickness: 50 nm) [18,19], which will be useful as a seed layer for a thick (> 500 nm) light absorbing layer. Research on ALILE of Si [24–31] has a longer history than that of Ge, and therefore, the 'seed layer concept' using ALILE-Si has been well studied [32–34], resulting in excellent thin-film solar cells [35–42]. In this study, we adopted the Ge layer formed by ALILE as an epitaxial seed of a high-quality light absorption layer. The resulting Ge layer, formed by solid-phase epitaxy (SPE), exhibited a long minority carrier lifetime, comparable to that of a bulk Ge

substrate.

II. EXPERIMENT

The 50-nm-thick Ge seed layer on the glass substrate was prepared using ALILE (Fig. 1(a)). In the ALILE process, 50-nm-thick Al and 75-nm-thick a-Ge thin films were sequentially prepared onto a quartz glass (SiO_2) substrate at room temperature using radiofrequency (RF) magnetron sputtering (base pressure: 3×10^{-4} Pa) with an Ar sputtering pressure of 0.2 Pa and an RF power of 50 W. The deposition rate was 28 nm/min for Ge and 31 nm/min for Al. An AlO_x layer between the Al and a-Ge layers was prepared by air exposure (5 min). The sample was annealed at 350 °C for 100 h in N_2. After annealing, the sample was treated by an H_2O_2 (50%) solution for 30 min to remove "Ge islands", followed by an HF solution (1.5%) for 1 min to remove Al and AlO_x layers [18]. These etching were processed at room temperature without agitation. Then, Ge layers were grown on the ALILE-Ge seed layer by molecular beam epitaxy (MBE) or SPE. For both methods, the Ge atoms were supplied by a Knudsen cell in an MBE system (base pressure: 5×10^{-7} Pa) at a deposition rate of 1.0 nm/min. For the MBE, Ge layers were deposited for 500 min at the growth temperature, T_g, ranging from 200 to 650 °C. For the SPE, a-Ge layers were deposited at room temperature for 100−500 min. The a-Ge samples were then annealed at T_g ranging from 300 to 500 °C for 50 h in a N_2 ambient. The crystal quality of the samples was evaluated using scanning electron microscopy (SEM), electron backscatter diffraction (EBSD), Raman spectroscopy (wavelength 532 nm), and secondary ion mass spectroscopy (SIMS). The light absorption coefficient α and the effective minority carrier lifetime τ_{eff} of the samples were evaluated using transmittance measurement and microwave photoconductivity decay (μ-PCD; excitation wavelength 349 nm, microwave frequency 26 GHz), respectively.

III. RESULTS AND DISCUSSION

Figure 1(b) and (c) show the EBSD images in the normal direction (ND) and (c) transverse direction (TD), corresponding to the crystal orientation in the out-of-plane and in-plane directions, respectively. These images show that the ALILE-Ge seed layer is highly (111)-oriented and large-grained (> 100 µm). These are the typical features of ALILE-Ge, especially owing to the AlO_x diffusion controlling layer and low temperature annealing [15]. Figure 2(a) shows that the Ge peaks of the MBE samples are sharp and present at 300 cm^{-1}, corresponding to crystalline (c-) Ge [11], while the Ge peak of the seed layer is broadly shifted to the lower wavenumber, likely due to high Al concentration (4×10^{20} cm^{-3}) [17]. These results suggest that the deposited Ge layers are crystalline and contain fewer Al atoms than the seed layer. Figure 2(b) and (f) show that the T_g = 200 °C sample has only a small area of (111) orientation and is small-grained, respectively. These results clearly indicate that epitaxial growth is incomplete. In contrast, Fig. 2(c)–(e) and (g)–(i) show that the samples for $T_g \geq 350$ °C exhibit high (111) orientation and large grains, respectively. These results suggest the epitaxial growth of Ge from the ALILE-Ge seed layer. Figure 2(j) shows that the Ge surface for T_g = 200 °C is almost flat, although there are voids originating from the seed layer [18]. However, Fig. 2(k)–(m) show that the Ge layer becomes discontinuous and island-shaped as T_g increases. This is the typical feature of MBE growth from the (111) oriented seed layer, which can be explained from the anisotropy of the growth rate. Because the growth rate of the (111) plane is the slowest [43], other planes appear during the growth, resulting in the rough surface. Thus, under the current growth conditions, epitaxial growth of a flat continuous MBE-Ge layer on the ALILE-Ge seed layer was difficult.

Figure 3(a) shows that the closer the epi-Ge/ALILE-Ge interface, the higher the Al concentration in the epi-Ge layer, which is more prominent as T_g is higher. Figure 3(b) shows that the Al concentration of the MBE-Ge layers, determined by the SIMS profiles at 100 nm

depth, are lower than that of the ALILE-Ge seed layer. The Al concentration decreases to the order of 10^{17} cm^{-3} by lowering T_g. These results are consistent with the fact that the diffusion coefficient of impurities increases with increasing temperature [44]. Figure 3(c) shows that the MBE-Ge samples exhibit much faster decay than the ALILE-Ge. By defining τ_{eff} as the time until the microwave intensity decays to $1/e$, τ_{eff} of the MBE-Ge layers is determined to be 8 ns. This value is around the detection limit of the μ-PCD system and is lower than τ_{eff} of the ALILE-Ge (67 ns). Therefore, the deterioration of τ_{eff} is likely attributed to the surface carrier recombination due to the rough surface of the MBE-Ge layers. The MBE-Ge layers thus achieved an Al concentration three orders of magnitude lower than ALILE by lowering T_g; however, there was a problem of islandization significantly degrading τ_{eff}.

To solve the degrading islandization problem, we investigated the SPE of Ge from the ALILE-Ge seed layer. Figure 4(a) shows that the SPE-Ge layer crystallizes at $T_g > 300$ °C. Considering that nucleation in a-Ge requires at least 375 °C [11], the $T_g = 350$ °C sample likely crystallizes from the seed layer. Figure 4(b)–(e) show that the crystal orientation map of the SPE-Ge layer greatly varies depending on T_g. According to the correspondence with the Raman results, the $T_g = 300$ °C sample is amorphous (Fig. 4(b) and (f)) and the $T_g = 500$ °C sample is microcrystalline, likely due to the bulk nucleation (Fig. 4(e) and (i)). The $T_g = 350$ °C sample is highly (111)-oriented and large-grained (Fig. 4(c) and (g)), indicating the epitaxial growth from the seed layer. Although the $T_g = 450$ °C sample seems to have epitaxially grown partially from the seed layer, there are also many randomly oriented grains due to bulk nucleation (Fig. 4(d) and (h)). Thus, only the $T_g = 350$ °C sample perfectly inherits the (111)-orientation and large grains of the seed layer. The SEM images in Fig. 4(j)–(m) show that, although there are indentations corresponding to the holes in the ALILE-Ge layer [18], the SPE-Ge surface is continuous and much flatter than the MBE-Ge surface regardless of T_g.

The optical properties of the SPE-Ge for $T_g = 350$ °C was evaluated. Figure 5 (a) shows

that α of SPE-Ge is the same as that of conventional undoped poly-Ge directly formed on a glass substrate at 350 °C. This result indicates that the SPE-Ge is low Al doped and not degenerated. From the α spectrum, the penetration depth of μ-PCD laser in SPE-Ge is found to be approximately 100 nm. Figure 5(b) shows that the μ-PCD decay curve depends on the thickness of the SPE-Ge layer. Figure 5(c) shows that the SPE-Ge samples appear larger $\tau_{\rm eff}$ than the ALILE-Ge. In addition, $\tau_{\rm eff}$ increases with the increasing thickness of SPE-Ge, w. The SPE-Ge for w = 500 nm achieves $\tau_{\rm eff}$ of more than 1 μs, exceeding that of the MBE-Ge by two orders of magnitude. In general, $\tau_{\rm eff}$ includes the contributions of bulk, surface, and interface recombination. When the minority carrier diffusion length is sufficiently larger than w, $\tau_{\rm eff}$ can be expressed as

$$\frac{1}{\tau_{\rm eff}} = \frac{1}{\tau_{\rm bulk}} + \frac{S_0 + S_{\rm w}}{w}, \tag{1}$$

where $\tau_{\rm bulk}$ is the bulk minority carrier lifetime, and S_0 and $S_{\rm w}$ are the surface and interface recombination velocities, respectively. Figure 5(d) shows that $1/\tau_{\rm eff}$ is proportional to $1/w$, indicating $\tau_{\rm eff}$ of the SPE samples is limited by the surface and/or interface recombination. The value of $S_0 + S_{\rm w}$ was determined to be 38 cm/s. Therefore, the passivation of the surface and/or interface is essential for improving $\tau_{\rm eff}$. From the intercept of the least-squares line in Fig. 5(c), $\tau_{\rm bulk}$ is determined to be 5.6 μs. This value is close to that of a single-crystal Ge with hole concentration in the latter half of 10^{17} cm^{-3} [45]. SIMS measurement revealed that the amount of Al in the SPE-Ge layer for $T_{\rm g}$ = 350 °C was 6×10^{17} cm^{-3}, almost the same as that of the MBE-Ge layer for $T_{\rm g}$ = 350 °C. Assuming that the Al atoms in the SPE-Ge are fully activated as acceptors, $\tau_{\rm bulk}$ of the SPE-Ge is mostly limited by impurity scattering. Therefore, further reducing the Al concentration in the SPE-Ge will lead to the further improvement of $\tau_{\rm bulk}$.

IV. CONCLUSION

The large-grained, highly (111)-oriented Ge layer formed by ALILE worked well as an

epitaxial seed layer for a high-quality Ge layer. After examining MBE and SPE for both methods, 500-nm-thick epitaxial Ge layers with an Al concentration of the order of 10^{17} cm^{-3} were obtained at T_g = 350 °C. The MBE-Ge layer exhibited a short τ_{eff} (8 ns) owing to the rough surface, while the flat SPE-Ge layer exhibited a long τ_{eff} (1.1 μs). Moreover, τ_{bulk} of the SPE-Ge layer was determined to be 5.6 μs, which is close to that of a single-crystal Ge. This achievement will directly lead to the fabrication of novel high-efficiency multijunction solar cells based on inexpensive substrates.

ACKNOWLEDGEMENTS

This work was financially supported by the JSPS KAKENHI (No. 26709019; No. 17H04918), the Asahi Glass Foundation, and the Nanotech CUPAL. Some experiments were conducted at the International Center for Young Scientists in NIMS and the Nanotechnology Platform in the University of Tsukuba. The authors are grateful to Professor N. Usami at Nagoya University and Dr. K. Hara at the University of Yamanashi for assistance with the μ-PCD measurement.

REFERENCES

[1] R.R. King, D.C. Law, K.M. Edmondson, C.M. Fetzer, G.S. Kinsey, H. Yoon, R.A. Sherif, N.H. Karam, 40% efficient metamorphic GaInP/GaInAs/Ge multijunction solar cells, Appl. Phys. Lett. 90 (2007) 183516. doi:10.1063/1.2734507.

[2] D. Shahrjerdi, S.W. Bedell, C. Ebert, C. Bayram, B. Hekmatshoar, K. Fogel, P. Lauro, M. Gaynes, T. Gokmen, J. a. Ott, D.K. Sadana, High-efficiency thin-film InGaP/InGaAs/Ge tandem solar cells enabled by controlled spalling technology, Appl. Phys. Lett. 100 (2012) 053901. doi:10.1063/1.3681397.

[3] M.G. Mauk, J.R. Balliet, B.W. Feyock, Large-grain (1-mm), recrystallized germanium films on alumina, fused silica, oxide-coated silicon substrates for III–V solar cell applications, J. Cryst. Growth. 250 (2003) 50–56. doi:10.1016/S0022-0248(02)02213-3.

[4] R. Takabe, S. Yachi, D. Tsukahara, K. Toko, and T. Suemasu, Growth of $BaSi_2$ continuous films on Ge(111) by molecular beam epitaxy and fabrication of p-$BaSi_2$/n-Ge heterojunction solar cells, Jpn. J. Appl. Phys. 56 (2017) 05DB02.

[5] K. Toko, M. Nakata, W. Jevasuwan, N. Fukata, T. Suemasu, Vertically Aligned Ge Nanowires on Flexible Plastic Films Synthesized by (111)-Oriented Ge Seeded Vapor-Liquid-Solid Growth, ACS Appl. Mater. Interfaces. 7 (2015) 18120–18124. doi:10.1021/acsami.5b05394.

[6] G. Taraschi, A.J. Pitera, E.A. Fitzgerald, Strained Si, SiGe, and Ge on-insulator: review of wafer bonding fabrication techniques, Solid. State. Electron. 48 (2004) 1297–1305. doi:10.1016/j.sse.2004.01.012.

[7] T. Maeda, H. Ishii, T. Itatani, E. Mieda, W. Jevasuwan, Y. Kurashima, H. Takagi, T. Yasuda, T. Takada, T. Yamamoto, T. Aoki, T. Osada, O. Ichikawa, M. Hata, Ultrathin layer transfer technology for post-Si semiconductors, Microelectron. Eng. 109 (2013) 133–136. doi:10.1016/j.mee.2013.03.069.

[8] E.U. Onyegam, D. Sarkar, M. Hilali, S. Saha, R. a. Rao, L. Mathew, D. Jawarani, J. Mantey, M. Ainom, R. Garcia, W. James, S.K. Banerjee, Exfoliated, thin, flexible germanium heterojunction solar cell with record FF=58.1%, Sol. Energy Mater. Sol. Cells. 111 (2013) 206–211. doi:10.1016/j.solmat.2013.01.002.

[9] K. Toko, I. Nakao, T. Sadoh, T. Noguchi, M. Miyao, Electrical properties of poly-Ge on glass substrate grown by two-step solid-phase crystallization, Solid. State. Electron. 53 (2009) 1159–1164. doi:10.1016/j.sse.2009.08.002.

[10] C.-Y. Tsao, J.W. Weber, P. Campbell, P.I. Widenborg, D. Song, M. a. Green, Low-temperature growth of polycrystalline Ge thin film on glass by in situ deposition and ex situ solid-phase crystallization for photovoltaic applications, Appl. Surf. Sci. 255 (2009) 7028–7035. doi:10.1016/j.apsusc.2009.03.035.

[11] K. Toko, R. Yoshimine, K. Moto, T. Suemasu, High-hole mobility polycrystalline Ge on an insulator formed by controlling precursor atomic density for solid-phase crystallization, Sci. Rep. 7 (2017) 16981. doi:10.1038/s41598-017-17273-6.

[12] C.-Y. Tsao, J.W. Weber, P. Campbell, G. Conibeer, D. Song, M. A. Green, In situ low temperature growth of poly-crystalline germanium thin film on glass by RF magnetron sputtering, Sol. Energy Mater. Sol. Cells. 94 (2010) 1501–1505.

[13] M. Tada, J.-H. Park, J.R. Jain, K.C. Saraswat, Low-Temperature, Low-Pressure Chemical Vapor Deposition and Solid Phase Crystallization of Silicon–Germanium Films, J. Electrochem. Soc. 156 (2009) D23. doi:10.1149/1.3008009.

[14] T. Matsui, C.W. Chang, T. Takada, M. Isomura, H. Fujiwara, M. Kondo, Thin film solar cells based on microcrystalline silicon–germanium narrow-gap absorbers, Sol. Energy Mater. Sol. Cells. 93 (2009) 1100–1102. doi:10.1016/j.solmat.2008.12.023.

[15] S. Hu, P.C. McIntyre, Nucleation and growth kinetics during metal-induced layer exchange crystallization of Ge thin films at low temperatures, J. Appl. Phys. 111 (2012) 044908. doi:10.1063/1.3682110.

[16] K. Toko, M. Kurosawa, N. Saitoh, N. Yoshizawa, N. Usami, M. Miyao, T. Suemasu, Highly (111)-oriented Ge thin films on insulators formed by Al-induced crystallization, Appl. Phys. Lett. 101 (2012) 072106.

[17] K. Toko, R. Numata, N. Oya, N. Fukata, N. Usami, T. Suemasu, Low-temperature (180 °C) formation of large-grained Ge (111) thin film on insulator using accelerated metal-induced crystallization, Appl. Phys. Lett. 104 (2014) 022106.

[18] K. Toko, K. Nakazawa, N. Saitoh, N. Yoshizawa, T. Suemasu, Improved Surface Quality of the Metal-Induced Crystallized Ge Seed Layer and Its Influence on Subsequent Epitaxy, Cryst. Growth Des. 15 (2015) 1535–1539. doi:10.1021/acs.cgd.5b00060.

[19] K. Toko, K. Kusano, M. Nakata, T. Suemasu, Low temperature synthesis of highly oriented p-type $Si_{1-x}Ge_x$ (x : 0–1) on an insulator by Al-induced layer exchange, J. Appl. Phys. 122 (2017) 155305. doi:10.1063/1.4996373.

[20] J.-H. Park, T. Suzuki, M. Kurosawa, M. Miyao, T. Sadoh, Nucleation-controlled gold-induced-crystallization for selective formation of Ge(100) and (111) on insulator at low-temperature (~250 °C), Appl. Phys. Lett. 103 (2013) 082102.

[21] H. Higashi, K. Kasahara, K. Kudo, H. Okamoto, K. Moto, J.-H. Park, S. Yamada, T. Kanashima, M. Miyao, I. Tsunoda, and K. Hamaya, A pseudo-single-crystalline germanium film for flexible electronics, Appl. Phys. Lett. 106 (2015) 041902.

[22] R. Yoshimine, K. Toko, N. Saitoh, N. Yoshizawa, T. Suemasu, Silver-induced layer exchange for polycrystalline germanium on a flexible plastic substrate, J. Appl. Phys. 122 (2017) 215305. doi:10.1063/1.5005002.

[23] T. Suzuki, B.M. Joseph, M. Fukai, M. Kamiko, K. Kyuno, Low-temperature (330 °C) crystallization and dopant activation of Ge thin films via AgSb-induced layer exchange: Operation of an n-channel polycrystalline Ge thin-film transistor, Appl. Phys. Express. 10 (2017) 095502. doi:10.7567/APEX.10.095502.

[24] O. Nast, T. Puzzer, L.M. Koschier, A.B. Sproul, S.R. Wenham, Aluminum-induced crystallization of amorphous silicon on glass substrates above and below the eutectic temperature, Appl. Phys. Lett. 73 (1998) 3214.

[25] M. Kurosawa, N. Kawabata, T. Sadoh, M. Miyao, Orientation-controlled Si thin films on insulating substrates by Al-induced crystallization combined with interfacial-oxide layer modulation, Appl. Phys. Lett. 95 (2009) 132103. doi:10.1063/1.3241076.

[26] A. Sarikov, J. Schneider, J. Berghold, M. Muske, I. Sieber, S. Gall, W. Fuhs, A kinetic simulation study of the mechanisms of aluminum induced layer exchange process, J. Appl. Phys. 107 (2010) 114318.

[27] B.I. Birajdar, T. Antesberger, B. Butz, M. Stutzmann, E. Spiecker, Direct in situ transmission electron microscopy observation of Al push up during early stages of the Al-induced layer exchange, Scripta Materialia 66 (2012) 550.

[28] Z. Wang, J. Wang, L. Jeurgens, E. Mittemeijer, Tailoring the Ultrathin Al-Induced Crystallization Temperature of Amorphous Si by Application of Interface Thermodynamics, Phys. Rev. Lett. 100 (2008) 125503. doi:10.1103/PhysRevLett.100.125503.

[29] R. Numata, K. Toko, N. Saitoh, N. Yoshizawa, N. Usami, T. Suemasu, Orientation Control of Large-Grained Si Films on Insulators by Thickness-Modulated Al-Induced Crystallization, Cryst. Growth Des. 13 (2013) 1767–1770. doi:10.1021/cg4000878.

[30] K. Toko, R. Numata, N. Saitoh, N. Yoshizawa, N. Usami, T. Suemasu, Selective formation of large-grained, (100)- or (111)-oriented Si on glass by Al-induced layer exchange, J. Appl. Phys. 115 (2014) 094301. doi:10.1063/1.4867218.

[31] S. Tutashkonko, N. Usami, Effects of the Si/Al layer thickness on the continuity, crystalline orientation and the growth kinetics of the poly-Si thin films formed by aluminum-induced crystallization, Thin Solid Films. 616 (2016) 213–219. doi:10.1016/j.tsf.2016.08.016.

[32] W. Fuhs, S. Gall, B. Rau, M. Schmidt, J. Schneider, A novel route to a polycrystalline silicon thin-film solar cell, Sol. Energy. 77 (2004) 961–968. http://www.sciencedirect.com/science/article/pii/S0038092X04001021.

[33] Y. Ishikawa, A. Nakamura, Y. Uraoka, T. Fuyuki, Polycrystalline Silicon Thin Film for Solar Cells Utilizing Aluminum Induced Crystallization Method, Jpn. J. Appl. Phys. 43 (2004) 877–881. doi:10.1143/JJAP.43.877.

[34] B.-R. Wu, S.-Y. Lo, D.-S. Wuu, S.-L. Ou, H.-Y. Mao, J.-H. Wang, R.-H. Horng, Direct growth of large grain polycrystalline silicon films on aluminum-induced crystallization seed layer using hot-wire chemical vapor deposition, Thin Solid Films. 520 (2012) 5860–5866. doi:10.1016/J.TSF.2012.05.009.

[35] A.G. Aberle, A. Straub, P.I. Widenborg, A.B. Sproul, Y. Huang, P. Campbell, Polycrystalline silicon thin-film solar cells on glass by aluminium-induced crystallisation and subsequent ion-assisted deposition (ALICIA), Prog. Photovoltaics Res. Appl. 13 (2005) 37–47.

doi:10.1002/pip.577.

[36] I. Gordon, L. Carnel, D. Van Gestel, G. Beaucarne, J. Poortmans, 8% Efficient thin-film polycrystalline-silicon solar cells based on aluminum- induced crystallization and thermal CVD, Prog. Photovoltaics Res. Appl. 15 (2007) 575–586. doi:10.1002/pip.765.

[37] S. Gall, C. Becker, E. Conrad, P. Dogan, F. Fenske, B. Gorka, K.Y. Lee, B. Rau, F. Ruske, B. Rech, Polycrystalline silicon thin-film solar cells on glass, Sol. Energy Mater. Sol. Cells. 93 (2009) 1004–1008. doi:10.1016/j.solmat.2008.11.029.

[38] Ö. Tüzün, Y. Qiu, A. Slaoui, I. Gordon, C. Maurice, S. Venkatachalam, S. Chatterjee, G. Beaucarne, J. Poortmans, Properties of n-type polycrystalline silicon solar cells formed by aluminium induced crystallization and CVD thickening, Sol. Energy Mater. Sol. Cells. 94 (2010) 1869–1874. doi:10.1016/j.solmat.2010.06.031.

[39] S. He, J. Janssens, J. Wong, A.B. Sproul, The influence of base doping density on the performance of evaporated poly-Si thin-film solar cells by solid-phase epitaxy, Thin Solid Films. 519 (2010) 475–478. doi:10.1016/j.tsf.2010.07.116.

[40] C. Jaeger, T. Matsui, M. Takeuchi, M. Karasawa, M. Kondo, M. Stutzmann, Thin Film Solar Cells Prepared on Low Thermal Budget Polycrystalline Silicon Seed Layers, Jpn. J. Appl. Phys. 49 (2010) 112301. doi:10.1143/JJAP.49.112301.

[41] D. Van Gestel, I. Gordon, J. Poortmans, Aluminum-induced crystallization for thin-film polycrystalline silicon solar cells: Achievements and perspective, Sol. Energy Mater. Sol. Cells. 119 (2013) 261–270. doi:10.1016/j.solmat.2013.08.014.

[42] W. Li, S. Varlamov, M. Jung, J. Huang, Vapour-Phase and Solid-Phase Epitaxy of Silicon on Solid-Phase Crystallised Seed Layers for Solar Cells Application, Int. J. Photoenergy. 2014 (2014) 1–9. doi:10.1155/2014/234602.

[43] L. Csepregi, R.P. Küllen, J.W. Mayer, T.W. Sigmon, Regrowth kinetics of amorphous Ge layers created by 74Ge and 28Si implantation of Ge crystals, Solid State Commun. 21 (1977) 1019–1021. doi:10.1016/0038-1098(77)90009-6.

[44] J. Räisänen, Annealing behaviour of aluminium implanted germanium, Solid. State. Electron. 25 (1982) 49–54. doi:10.1016/0038-1101(82)90093-4.

[45] E. Gaubas, J. Vanhellemont, Dependence of carrier lifetime in germanium on resisitivity and carrier injection level, Appl. Phys. Lett. 89 (2006) 142106. doi:10.1063/1.2358967.

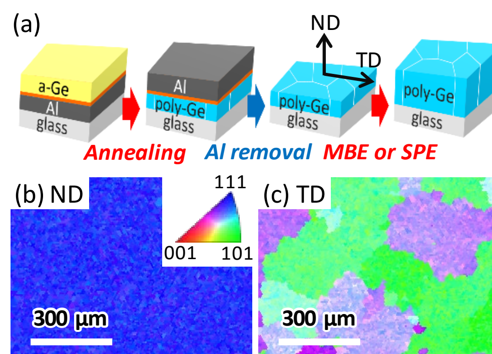

Fig. 1. (a) Schematic of the sample preparation. EBSD images of an ALILE-Ge seed layer in the (b) ND and (c) TD. The coloration indicates the crystal orientation, refer to the inserted legend.

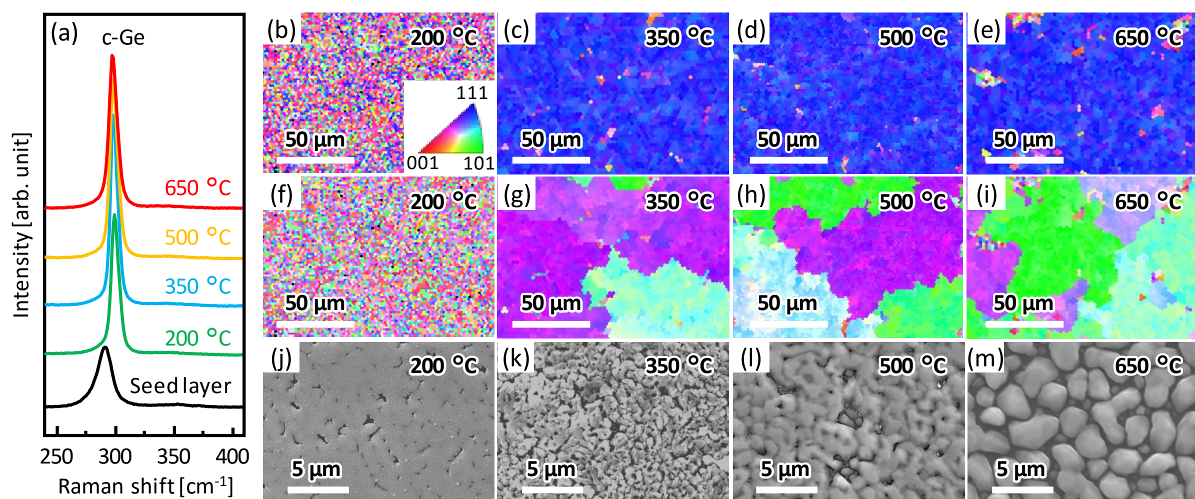

Fig. 2. Characterization of the crystal quality of the samples for MBE where T_g = 200−650 °C. (a) Raman spectra where the data of the seed layer is shown for comparison. EBSD images in (b)−(e) ND and (f)−(i) TD. (j)−(m) SEM images. T_g is labeled in each image.

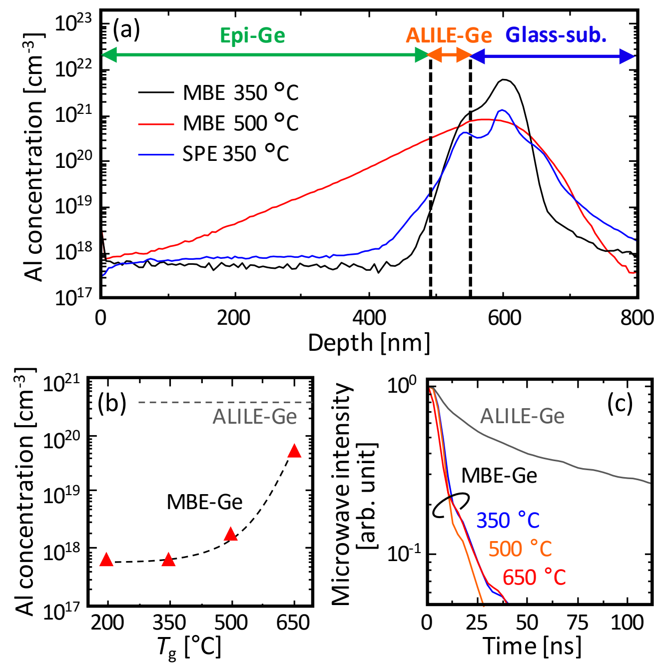

Fig. 3. (a) SIMS depth profiles of Al concentration in the epi-Ge layers formed by MBE (T_g = 350 and 500 °C) and SPE (T_g = 350 °C). (b) T_g dependence of Al concentration in the MBE-Ge layers obtained by SIMS analyses. (c) Normalized μ-PCD decay curves for the MBE samples where T_g = 350, 500, and 650 °C. The data for the ALILE-Ge seed layer are shown for comparison.

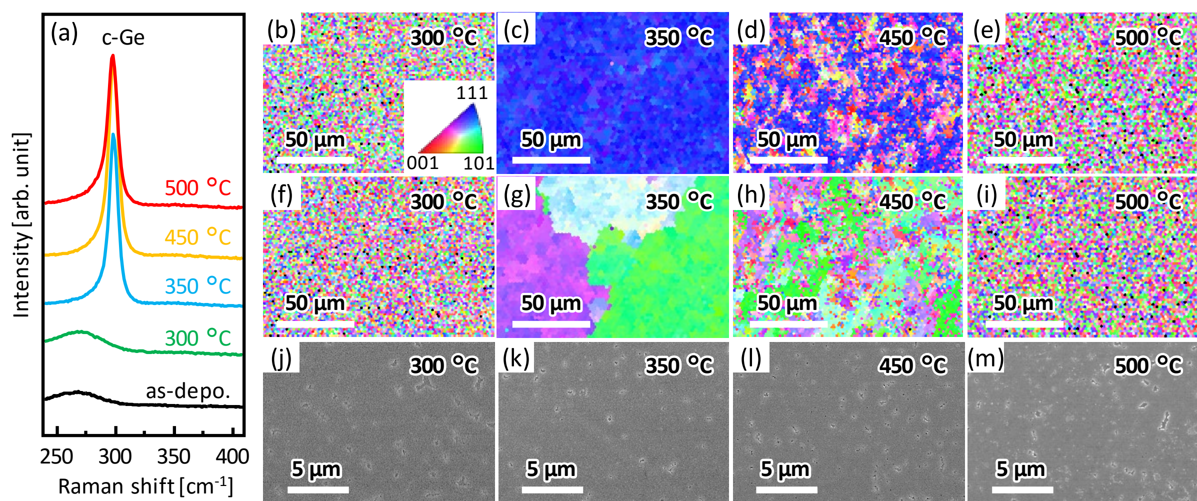

Fig. 4. Characterization of the crystal quality of the samples for SPE where T_g = 300−500 °C. (a) Raman spectra where the data of the seed layer is shown for comparison. EBSD images in (b)−(e) ND and (f)−(i) TD. (j)−(m) SEM images. T_g is labeled in each image.

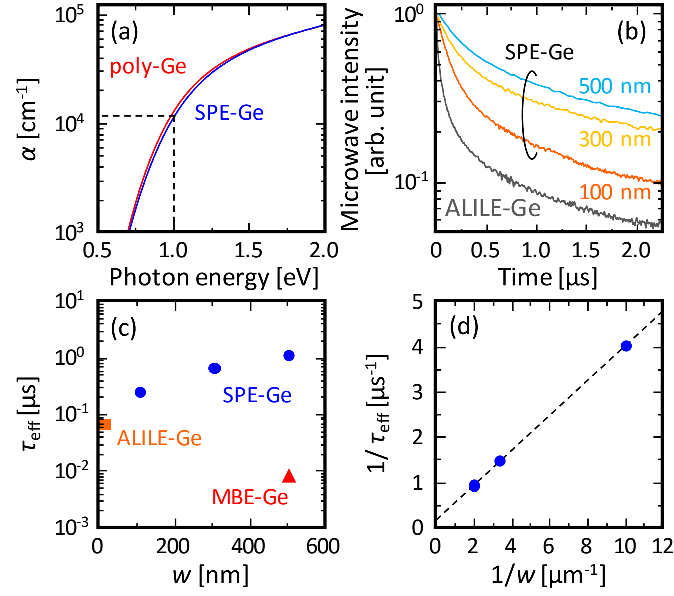

Fig. 5. Optical properties of the SPE-Ge for T_g = 350 °C. (a) α spectra of the SPE-Ge and conventional undoped poly-Ge samples where w is 500 nm. (b) Normalized μ-PCD decay curves of the SPE samples where w is 100, 300, and 500 nm. The data of the ALILE-Ge are shown for comparison. (c) τ_{eff} of the SPE-Ge layers as a function of w. The data of the ALILE-Ge and MBE-Ge are shown for comparison. (d) Dependence of the inverse of τ_{eff} on the inverse of w, including a dotted line fitted with three points.